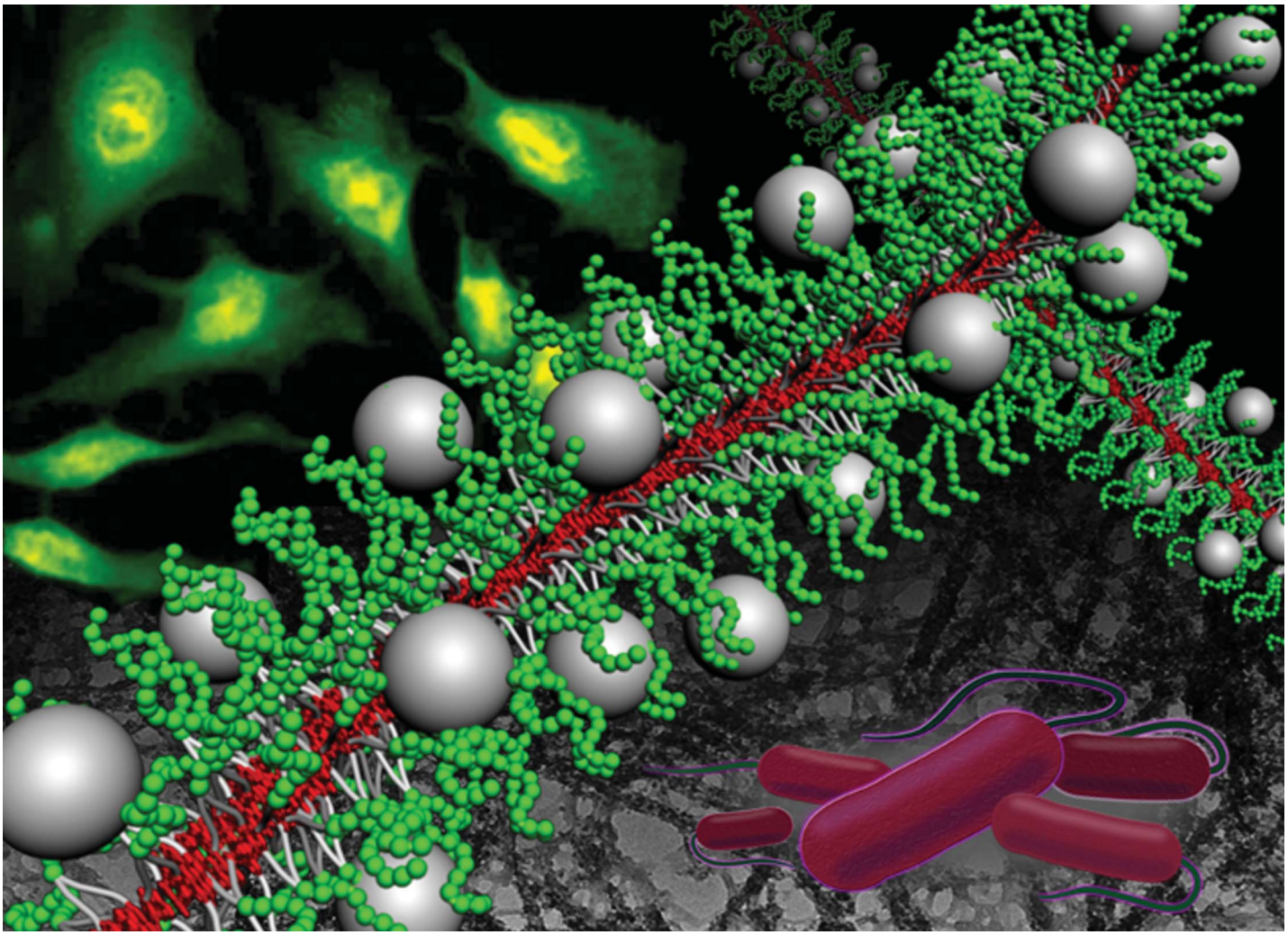

Showcasing research from Prof. Eunji Lee's laboratory, Graduate School of Analytical Science and Technology, Chungnam National University, Republic of Korea.

Title: A "Light-up" 1D supramolecular nanoprobe for silver ions based on assembly of pyrene-labeled peptide amphiphiles: cell-imaging and antimicrobial activity

The histidine-coated fibrillar nanoprobe response to Ag^+ with fluorescence enhancement was developed through a rational design based on the aqueous self-assembly of peptide amphiphiles for potential use as cell-imaging and antimicrobial agents.

As featured in:

See Eunji Lee *et al.*, *J. Mater. Chem. B*, 2014, **2**, 6478.

ROYAL SOCIETY OF CHEMISTRY

www.rsc.org/MaterialsB

Registered charity number: 207890

Journal of Materials Chemistry B

PAPER

View Article Online
View Journal | View Issue

Cite this: J. Mater. Chem. B, 2014, 2, 6478

A "Light-up" 1D supramolecular nanoprobe for silver ions based on assembly of pyrene-labeled peptide amphiphiles: cell-imaging and antimicrobial activity†

Inhye Kim,[a] Heon-Ho Jeong,[b] Yong-Jae Kim,[a] Na-Eun Lee,[a] Kang-moo Huh,[c] Chang-Soo Lee,[b] Geon Hee Kim[ad] and Eunji Lee*[ad]

Received 3rd June 2014
Accepted 15th July 2014

DOI: 10.1039/c4tb00892h

www.rsc.org/MaterialsB

We prepared pyrene-labeled peptide amphiphiles (PAs) consisting of a hydrophobic linear- or branched-alkyl chain (for **1** or **2**, respectively) and a hydrophilic histidine-rich peptide of HGGGHGHGGGHG (HG12). Both peptides have a strong tendency to form nanofibrils (NFs) in aqueous media. The resulting histidine-coated NFs show a great binding affinity to Cu^{2+} as a fluorescence "light-off" sensor. Interestingly, the emission spectra of the pyrene probe show that the different supramolecular assemblies between **1** and **2** can significantly affect the binding affinity to specific metal ions. In particular, "light-up" fluorescent Ag^{+} detection of NFs of **2** through inhibition of photoinduced electron transfer (PET) was observed even at a low concentration of PA solution. As a means to determine the biological responsibility of **2** to Ag^{+}, intracellular detection using the "turn-on" response was performed. A considerable enhancement of fluorescence in NF-loaded HeLa cells was observed. In addition, the NFs were used as a template scaffold for the production of Ag nanoparticles (AgNPs) with high monodispersity and stability. The NFs decorated with AgNPs are shown to possess highly effective and long-term antibacterial activity against both Gram-negative and -positive bacteria.

Introduction

The self-assembly of peptide-conjugated amphiphiles (PAs) can lead to a variety of nanoarchitectures such as micelles, barrels, vesicles, nanofibrils (NFs), ribbons and tubes, in aqueous media.[1] They have been recognized as some of the most attractive biomaterial scaffolds due to their inherent properties including good biodegradability, biocompatibility and bioactivity.[2] Understanding the self-assembly process of naturally and rationally designed PAs and the resulting well-organized nanostructures at the molecular level has created new opportunities for developing novel functional materials for applications such as tissue engineering,[3] regenerative medicine,[4] targeted therapeutic delivery[5] and diagnosis.[6] For instance, among the PA-based nanostructures, one-dimensional (1D) β-sheet rich fibrillar assemblies of PAs have been known to play a central role in neurodegenerative disease which give rise to not only a functional motif for biomedical materials,[7,8] but also a structural diversity for the 1D assembly of nanomaterials.[9] In addition, the intrinsic propensity of PAs to form core–shell aggregates in aqueous solutions allows for the easy addition of desired chemical and biological activities to the specific region of the nanostructure by incorporating a functional building block into the molecular architecture.[10–13] However, NFs with optical responses to the physiological environment, as a result of changing the molecular packing within the fibrillar core, have rarely been investigated.[14,15]

Meanwhile, the molecular systems used to capture metal ions with biological interest have been intensively investigated and applied in many fields, including diagnosis and clinical toxicology.[16,17] Among the peptide building blocks, histidine-rich peptides have attracted much attention as molecular recognition scaffolds for binding metal ions in the active sites of proteins due to a very efficient imidazole-nitrogen donor atom in the histidyl residue.[18] In particular, it has been reported that an HGGGHGHGGGHG (HG12) sequence consisting of histidine and glycine immobilized on the pre-assembled nanotube can complex with Cu^{2+} and Ni^{2+},[19] leading to the formation of metal nanoparticle-coated nanotubes in the presence of a reducing

[a]Graduate School of Analytical Science and Technology, Chungnam National University, Daejeon 305-764, Republic of Korea. E-mail: eunjilee@cnu.ac.kr; Fax: +82 42 821 8541; Tel: +82 42 821 8548

[b]Department of Chemical Engineering, Chungnam National University, Daejeon 305-764, Republic of Korea

[c]Department of Polymer Engineering, Chungnam National University, Daejeon 305-764, Republic of Korea

[d]Center for Analytical Instrumentation Development, Korea Basic Science Institute, Daejeon 305-806, Republic of Korea

† Electronic supplementary information (ESI) available: Detailed synthetic and experimental procedures. See DOI: 10.1039/c4tb00892h

agent.[20,21] This result stimulated us to investigate whether the introduction of HG12 into a hydrophilic block of PA would facilitate the utilization of self-assembled NFs as supramolecular platforms for the selective and sensitive detection of metal ions as well as for the nucleation and growth of metal crystals in aqueous solutions. It might ultimately be used to control the optoelectronic, magnetic, and biological properties of organic–inorganic NF-hybrids mimicking biomineralization.[22,23]

Along this line, HG12-conjugated PA **1** was simply designed, which contains a linear alkyl chain (Scheme 1). The pyrene moiety was attached to the N-terminus of **1** as a fluorescent probe to monitor the self-organization process of the PAs.[24] It has been well-known that the emission spectra of pyrene represent the relative spatial proximity between neighboring pyrene chromophores, which leads to the formation of a monomer or an excimer, enabling the interpretation of the molecular packing of the hydrophobic core in self-assembled nanostructures.[25] In order to promote the robust assembly of PAs through the enhanced hydrophobic interaction, a branched alkyl chain with a pyrene pendant was incorporated into PA **2**.[26]

Interestingly, although both **1** and **2** self-assembled into 1D NFs in an aqueous solution, they showed different molecular packing modes for pyrene (Fig. 1). The ability of the NFs to bind the specific metal ions was shown to work differently with respect to the spatial constraint of HG12 imposed by the molecular packing in the core of the NFs. More interestingly, the NFs of **2** exhibited a significant fluorescence "light-up" response to Ag^+. In general, efficient fluorescent chemosensors for metal ions were designed and developed based on various photoinduced processes,[27] but most of the pyrene fluorophore-containing supramolecular systems have shown fluorescence quenching *via* electron or energy transfer, leading to low sensitivity.[28] In addition, silver-containing nanomaterials have been of special interest due to their low toxicity toward mammalian cells, strong antimicrobial activity against bacteria, and unique optical properties.[29] For this reason, one can envision that the supramolecular fibrils decorated with Ag^+ by fluorescence "light-up" molecular recognition in an aqueous solution can act as both a multifunctional nanoplatform for developing a highly sensitive supramolecular probe for metal ion detection in live cells and an antimicrobial agent leading to potent long-lasting activity.

Herein, we report the unique self-assembling characteristics of PAs to form NFs depending on the nature of alkyl chains (*i.e.*, a linear or branched structure of the chains). The NFs are coated with a metal-binding peptide that showed a great binding affinity to Cu^{2+}, leading to the fluorescence "light-off" response.

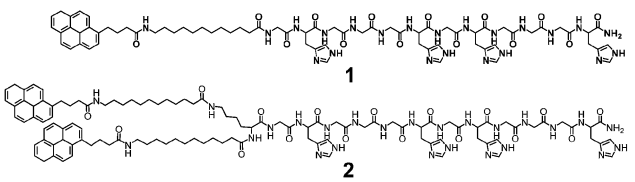

Scheme 1 Molecular structures of PAs **1** and **2**.

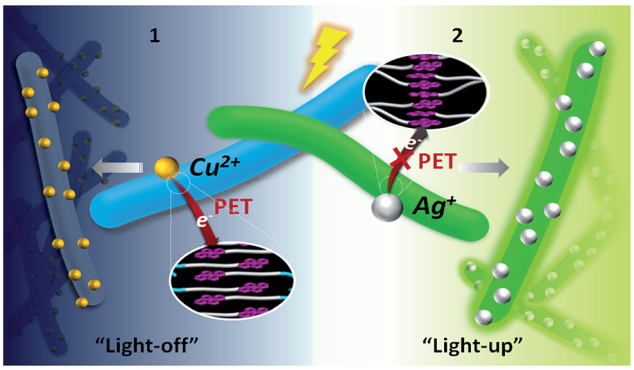

Fig. 1 Schematic representation of the formation of "light-off" and "light-on" fluorescent 1D nanoprobes in response to copper and silver ions, depending on the molecular assembly of the pyrene-labeled PAs **1** and **2**, respectively.

Remarkably, the ability of the NFs to bind Ag^+ enables the intracellular imaging of HeLa cells by the fluorescence "turn-on" response and the fabrication of Ag nanoparticles (AgNPs) on the surface of NFs by the reduction of Ag^+ with $NaBH_4$. The resulting AgNP–NF hybrid system shows an effective antimicrobial effect against both Gram-negative and -positive bacteria. Most chemosensors for Ag^+ exhibit a limitation in practical biomedical applications due to the small molecule-based development, low sensitivity from the "turn-off" response, and low water solubility.[30] To the best of our knowledge, this report is the first example of supramolecular 1D nanoprobes showing dual functions: a "light-up" response for Ag^+ in an aqueous solution, and growth templates for AgNPs, leading to cell imaging and an antibacterial effect. It may provide a useful strategy for the fabrication of biomedical nanomaterials for sensing and imaging, and it could have a special value in terms of comprehending the biological functions of the metal–peptide system.

Results and discussion

Synthesis and self-assembly behavior of PAs in water

The PAs were synthesized on Rink amide MBHA resin using standard Fmoc (9-fluorenylmethoxycarbonyl) protocols (Scheme S1 and S2†). Pyrene butyric acid was covalently linked to the N-terminus of the HG12 peptide segment through linear- or branched-dodecanoic acid (C_{12}) tails.[31] The resulting crude product was purified to produce pure PAs (>95% as determined by analytical HPLC, Fig. S1†). The molecular weight was confirmed using matrix-assisted laser desorption/ionization time-of-flight (MALDI-TOF) mass spectroscopy, and it was consistent with the theoretical value (Fig. S1†).

To investigate the self-assembly behaviors of the PAs, transmission electron microscopy (TEM) experiments were performed on the aqueous solutions of PAs **1** and **2** (Fig. 2a–d). Direct visualization of the aggregates of PA **1** containing a linear-alkyl chain revealed micrometer-long NFs with regular diameters of 9.5 ± 1.0 nm (Fig. 2a and S4a†). Cryogenic TEM (cryo-TEM) experiments confirmed the presence of aqueous NFs

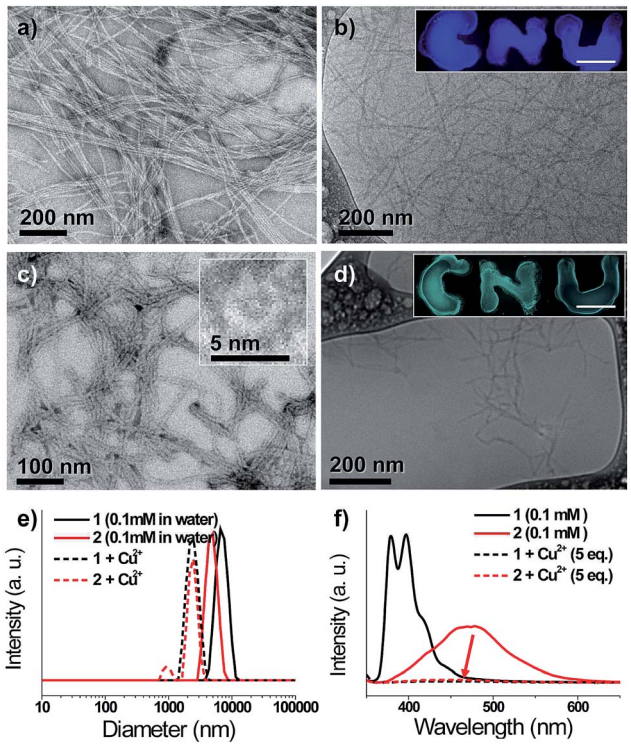

Fig. 2 Visualization of the aqueous self-assembled nanostructures of PAs; (a and c) negatively stained TEM and (b and d) cryo-TEM images of the NFs of **1** and **2**, respectively (inset: the fluorescent optical image, scale bars: 1 mm). (e) Hydrodynamic diameter and (f) emission spectra before and after the addition of Cu^{2+} to **1** and **2** (0.1 mM in water, λ_{ex} = 340 nm).

with an average diameter of 4.2 nm (Fig. 2b and S4b†). Normally, as the solvated hydrophilic block is invisible, the hydrophobic core appears to be dark in a cryo-TEM image.[32] Considering the extended molecular length of the hydrophobic block (*ca.* 2.8 nm by CPK modeling), the diameter of 4.2 nm is in reasonable agreement with the formation of interdigitated bilayer packing of **1** (Fig. S4e†).

Although **2** with a dibranched-alkyl chain is shown to form the NFs, the average diameters and lengths of the NFs decrease compared to those of **1** (Fig. 2c and d), which is consistent with the DLS data (Fig. 2e). The average hydrodynamic diameters (R_H) of **1** and **2** were 6.6 μm and 4.9 μm, respectively. Interestingly, the diameters of the NFs of **2** in TEM decreased to 8.2 ± 0.6 nm as compared with those in **1** (Fig. S4c†), whereas those in cryo-TEM increased to 5.7 nm (Fig. S4d†), averaged over 100 NFs. This unexpected increment in the diameter of the hydrophobic core, including the pyrenyl moiety and alkyl chains, is considered to be attributed to the change in the internal molecular packing with regard to the incorporation of the branched-dodecanoic tails. Fluorescence spectroscopy was first carried out to study the fine organization in the hydrophobic core of the NFs (Fig. 2f).[24,25] In an aqueous solution, PA **1** exhibited a strong monomer-like fluorescence band (λ_{em}, ~378 nm), while PA **2** showed an efficient excimer formation (λ_{em}, ~473 nm). These results give rise to a noticeable fluorescent color change in the solution from blue to green (inset of Fig. 2b and d). Since the fluorescence of a pyrene chromophore is highly sensitive to the local environment in self-assembled nanoaggregates,[24,25] it can be concluded that the PAs of **1** are interdigitated to form NFs in which pyrene tends to be intercalated between linear-alkyl chains, which corresponds to the existence of monomer-like emission of NFs.[14a]

In the case of PA **2** with dibranched-alkyl chains, a sandwich-like pyrene assembly is considered to be a contributing factor in the formation of the NFs.[12] It is the most probable packing structure in the fibrillar core (Fig. 1). In addition, the cross-sectional view of the NFs observed frequently in TEM studies provides an opportunity for greater understanding of the molecular organization of the NFs (inset of Fig. 2c and S4g†). It reveals that the molecular assembly of **2** favors a cylindrical geometry in which the diameter of the hydrophobic core is approximately 6 nm, which is consistent with the distance determined from cryo-TEM and computational modeling (Fig. S4†).[11] Unfortunately, the circular dichroism (CD) spectra of **1** and **2** show the presence of β-turn and β-sheet secondary structures, respectively,[33,34] based on the hydrogen bonding among the peptide segments in the aqueous solution, as opposed to random coils (Fig. S5†). Therefore, it is hard to demonstrate that the HG12 peptide block is fully hydrated.[15,32c] However, the difference (~2.5 nm) of the NF diameter of **2** between the TEM and cryo-TEM observations (~8.2 nm and 5.7 nm, respectively) and its excimer formation let us suppose that the NFs of **2** have close central packing between the pyrenyl groups, which results in the interdigitation of the PAs (Fig. 1). Although we are not aware of the exact arrangement of the hydrophobic alkyl chains in the fibrillar core, the incorporation of a bulky branched-alkyl chain would force an increase in the interfacial area between the hydrophobic alkyl chain and the HG12 peptide to avoid the unfavorable contact between the hydrophobic segment and water. The consequent relief from the steric constraint between the HG12 peptides, by changing from linear to branched alkyl chains, compensates for the strengthened aggregation between the pyrenyl groups and the β-sheet formation of peptides to barely maintain the aqueous assembly structure, which causes a decrease in the length of the NF. The appearance of a strong negative CD band of **2** near 240 nm, as compared to **1**, further proves the formation of a well-ordered pyrene structure in the NFs (Fig. S5†),[31] which corresponds with the fluorescence spectra showing the excimer formation (Fig. 2f). Therefore, it can be explained that the linear-alkyl chain-incorporated PA **1** shows conventional interdigitated bilayer assembly, while **2** reveals the unique bilayer packing arrangements in the NFs, as explained above.

Fluorometric "turn-off" sensing of the NFs for Cu^{2+} and the growth of CuNPs on the surface of the NFs

The metal ion recognition event of histidine-rich peptide (HG12) coated-NFs was first examined with Cu^{2+}.[20] The fibrillar structure with a high aspect ratio was maintained, while the fluorescence was significantly quenched following the addition of the paramagnetic d^9 Cu^{2+} (Fig. 2f and S7†).[35] In particular, λ_{max} of **2** was blue-shifted from 478 nm to 455 nm, indicating a

conversion of an excimer fashion from a sandwich-like dynamic excimer to a partially overlapped static excimer.[25,36] This means that a closer molecular interaction between the pyrenyl groups was induced by capturing of Cu^{2+} with the HG12. TEM images of the NFs of both **1** and **2** after the addition of Cu^{2+} reveal a remarkable enhancement of mass contrast even without staining (Fig. 3a and b). Indeed, the association between Cu^{2+} and the NFs was confirmed by MALDI-TOF/TOF MS.[37] In the presence of Cu^{2+}, the *m*/*z* values of the signals increased from that of the bare NFs (Fig. 3c). When a 5.0 equiv. of Cu^{2+} was added to the PA solutions, new signals appeared at 1553.8 *m*/*z* for **1** and 2127.1 *m*/*z* and 2136.0 *m*/*z* for **2**, in addition to the signals at 1491.9 *m*/*z* and 2089.0 *m*/*z*, respectively, which corresponded to $[\mathbf{1} - H + Cu(II)]^+$ for **1** and $[2\cdot\mathbf{2} + Cu(II) + H_2O]^+$ and $[2\cdot\mathbf{2} + Cu(II) + 2H_2O]^+$ for **2**. This indicates that the molar ratios of NF to Cu^{2+} for the complex are 1 : 1 and 2 : 1 for **1** and **2**, respectively, which are consistent with the stoichiometries found in the Job's plot analysis (Fig. S8c and S8f†).[38] Further evidence of Cu^{2+} binding on the NFs can be proved by Fourier transform infrared (FTIR) measurements, which monitor the N–H and C=C stretching vibrations in the imidazole side chain of histidine (Fig. 3d).[39] After the addition of Cu^{2+}, the ν_{N-H} at 3500 cm^{-1} was downshifted to 3490 cm^{-1} as the N–H bond elongated, while the $\nu_{C=C}$ at 1494 cm^{-1} was upshifted to 1508 cm^{-1} as the C=C bond shortened, suggesting chelation of the histidine residues

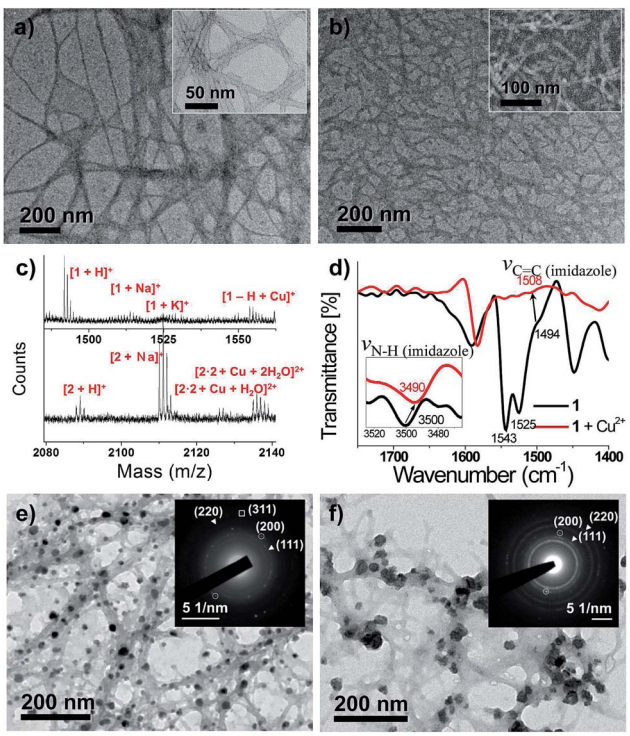

Fig. 3 The unstained TEM images of Cu^{2+}–NFs (0.1 mM) of (a) **1** and (b) **2** with enhanced contrast, respectively (inset, negatively stained images). (c) MALDI-TOF mass spectra of Cu^{2+}–PA complexes. (d) FTIR spectra before and after the addition of Cu^{2+} (inset, N–H stretching vibrations in the imidazole of the histidine). TEM images of the NFs decorated with CuNPs of (e) **1** and (f) **2**, respectively (inset, selected area diffraction patterns confirming the formation of Cu nanocrystals).

of HG12 with Cu^{2+}. And the amide II band of **1** at a 1543 cm^{-1} peak was significantly suppressed, indicating considerable destabilization of the β-turn structure of HG12.[18,19]

The formation of Cu^{2+}-coated NFs of **1** and **2** can be directly proved by the reduction in metal ions using $NaBH_4$. This leads to the formation of Cu nanocrystals.[20,40] The location of spherical NPs with a dark contrast on NFs with a grey contrast was observed in the TEM images (Fig. 3e and f). The average diameters of the CuNPs on both NFs **1** and **2** are 11.9 ± 2.6 nm and 21.6 ± 3.7 nm, respectively (Fig. S9†). The selected area electron diffraction (SAED) pattern of the resulting NPs shows (111), (200), (220), and (311) planes corresponding to a face-centered cubic crystal (inset of Fig. 3e and f).[41] Based on these results, we figure that the biocompatible hybrid NFs can be easily generated *via* the rational design of self-assembling PAs containing a metal-binding peptide segment to form the NF template, mimicking biomineralization.[23c]

Supramolecular fluorescent nanoprobe behavior of PAs to metal ions

To corroborate the metal-binding affinity of the aqueous NFs in detail, a variety of metal ions, including Ag^+, Ca^{2+}, Co^{2+}, Cu^{2+}, Fe^{2+}, Mg^{2+}, Mn^{2+}, Ni^{2+}, Pb^{2+}, and Zn^{2+}, were employed. These investigations may provide an opportunity to find interesting characteristics of the NFs. We first measured the critical micellar concentration (CMC) of **1** and **2** in water using a fluorescence spectrometer to systematically investigate the ability of the NFs as metal binders in a dilute solution. The intensity ratios of the two emission peaks (I_{396}/I_{378}) of the pyrene pendant were highly sensitive to the medium polarity, which was calculated and plotted against the concentration.[42] The CMCs of **1** and **2** were determined to be 7.5 μM and 6.1 μM, respectively (Fig. S10†). These low CMC values suggest that PAs can act as supramolecular 1D nanoprobes in a dilute condition. As expected, both PAs **1** and **2** were shown to self-assemble into NFs even at low concentrations close to the CMC (Fig. S11–S13†). The selectivity of probe **1** towards various metal ions was investigated at a concentration of 11.8 μM (Fig. S14†). The fluorescence emission of **1** decreased with an increase in the amount of metal ions *via* the photoinduced electron transfer (PET) mechanism.[43] In particular, Cu^{2+}, Ni^{2+}, and Fe^{2+}, according to the Irving–Williams series considerations,[44] caused a significant chelation-enhanced quenching effect (CHEQ),[45] which limits their application in sensing of the metal ions.

Remarkably, the fluorescence intensity of **2** in water (7.6 μM) progressively increased upon addition of Ag^+ (Fig. 4a). Cu^{2+} was the strongest quencher of fluorescence, whereas Ag^+ was the only metal ion that caused a significant emission enhancement in **2** (Fig. 4b). By adding Cu^{2+} to each metal solution, competition experiments clearly revealed that Ag^+ interferes with the binding and fluorescence quenching of **2** to Cu^{2+} (Fig. 4c). The stoichiometric ratio of **2** : Ag^+ was found to be 2 : 1 (inset of Fig. 4d). The incubation of PA **2** with $AgNO_3$ and the subsequent reduction with $NaBH_4$ led to the nucleation and growth of AgNPs along with the NFs, as shown in the TEM image in Fig. 4d. No negative staining was used, so the dark contrast of

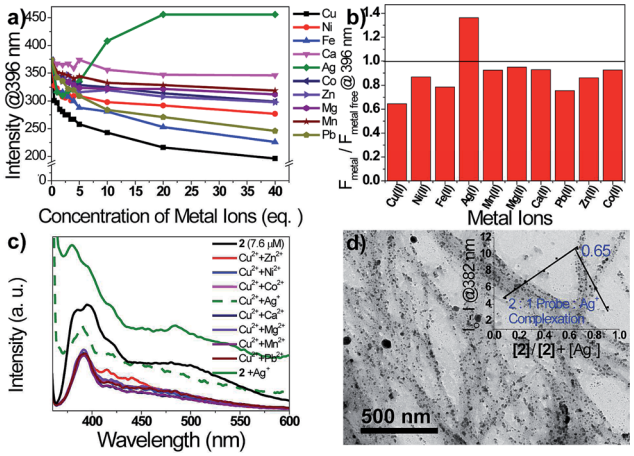

Fig. 4 (a) Fluorescence intensity of **2** (7.6 μM) upon the addition of various metal ions in water. (b) Fluorescence intensity ratios ($F_{metal}/F_{metal\ free}$) for **2** at 396 nm in the presence of 20 equiv. of specified metal ions. (c) Fluorescence spectra of **2** in response to the Cu^{2+} ions in the presence of various coexistent metal ions (λ_{ex} = 340 nm). (d) TEM image of AgNPs generated on the NFs of **2** (inset, fluorescence Job's plot for the determination of the stoichiometry of the NF **2**–Ag^+ complex).

the spherical aggregates was due to the AgNPs. Averaged over 50 AgNPs within the hybrid NFs, a diameter of 10.3 ± 1.7 nm was determined from the TEM images (Fig. S9†). These results demonstrated that the supramolecular fibril nanoprobe of **2** shows a selective fluorescence "light-up" detection of Ag^+ and the capability to transform into AgNP-incorporated hybrid NFs.

It is noted that the fluorescence emission spectrum of **2** changed at a low concentration to near the CMC of the PA solution, in contrast to **1** (Fig. S11†). When decreasing the concentration of **2** from 0.1 mM to 7.6 μM, the pyrene monomer-like emission appeared with excimer emission. The packing mode of the hydrophobic core with a centrally closed stack of pyrenyl groups seems to change to the interdigitation mode with the alkyl chains and pyrenyl groups facing each other, which satisfies the fibrillar thickness of ~6.5 nm in TEM and the monomer emission formation (Fig. S11†). It can be considered a plausible model for the hydrophobic cores in the NFs of **2**. Nevertheless, the NFs of **2** reveal an ability to form hybrid nanowires with AgNPs at both low and high concentrations (7.6 μM and 0.1 mM, Fig. S15†), indicating that the HG12 of NF **2** is a potent binding site of Ag^+ in a wide range of concentrations of the NF **2** solution. Therefore, the selective response of the NFs of **2** to Ag^+ can be understood by considering the packing arrangements of the PAs imposed by the molecular architecture. The PAs of **1** contain a hydrophobic block with a linear geometry, which are fully interdigitated with each other to avoid contact between the hydrophobic block and water, resulting in dense packing of the core. The incorporation of a bulky-branch shaped hydrophobic block into PA **2** hinders the dense packing within the core of the NF. These distinct differences were identified by FTIR spectroscopy (Fig. S16†). The IR bands at 2850 cm^{-1} and 2918 cm^{-1}, which correspond to symmetric and asymmetric stretching vibrations of CH_2, respectively, are sensitive to the crystalline packing of the alkyl chain.[15,46] The thin films of **1** cast from an aqueous solution show strong and sharp bands whereas the films of **2** represent weak and broad bands, indicating that the core of NFs of **2** has the less ordered "liquid-like" structure of alkyl chains.[15] As a result, the alleviation of the steric constraint between the HG12 blocks covalently attached to the end of the bulky branched alkyl chains, which results in loose distribution of HG12, offers enough space responsible for the binding of large metal ions on the exterior of the NFs. In conjunction with the fact that the radii of Cu^{2+}, Ni^{2+} (0.72 Å), and Fe^{2+} (0.76 Å) are comparable and that the radius of Ag^+ is larger (1.26 Å, Fig. S17†),[29a] the binding affinity of the NFs of **2** to Ag^+ can be rationalized by a great dependence on the packing density of HG12 and the space-filling requirement to metal ions in an aqueous solution. Consequently, the PAs with fluorophore–spacer–metal ion binding site architecture provide a fluorescence enhancement upon the binding event of Ag^+ to HG12 *via* the efficient inhibition of the PET process between the pyrene groups and HG12 (Fig. 1).[43a,47]

Dual functional fibrillar nanoprobe with Ag^+ detection: cell-imaging and antimicrobial activity

The formation of biocompatible PA-based NFs enables the pursuit of potential biomedical applications. Indeed, 10 μM of NF shows high cell viability (93%), which was evaluated by a standard live-dead assay of HeLa cells (Fig. S19†).[48] In particular, the selective response of NFs to Ag^+ with fluorescence emission enhancement stimulated the investigation into the abilities of PAs in cell-imaging.[49] The presence of Ag^+-immobilized nanofibers led to the investigation of whether the fabrication of hybrid NFs has the potential to induce antimicrobial effects (Fig. 5).[29,50] However, since it has been proven that AgNPs are more suitable antibacterial agents than substances based on the Ag^+ ion due to significantly lower toxicity toward mammalian cells,[51] the reduction process of Ag^+ attached to the surface of NFs was further performed.

Intact HeLa cells were incubated with 10 μM of **2** for 1 h in the absence of Ag^+ at 37 °C and then washed with 20 mM HEPES buffer solution (pH 6.8) containing $NaNO_3$ instead of NaCl, and

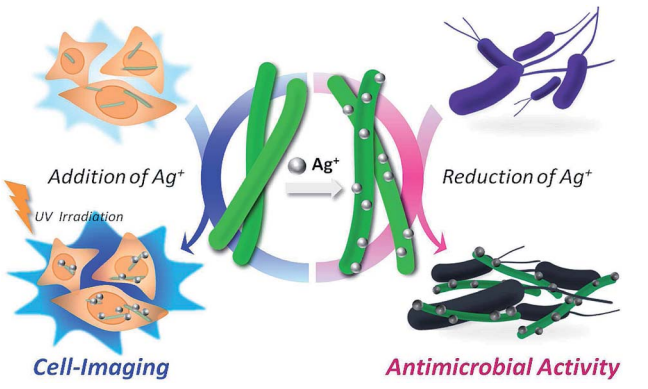

Fig. 5 Schematic representation of dual-functional hybrid PA-NFs for cell imaging and antimicrobial effects.

they exhibited weak intracellular fluorescence when monitored using fluorescence microscopy (Fig. 6b). It should be noted that the presence of Cl^- in the solution promotes the formation of $AgCl_{(s)}$, which interferes with the sensing of Ag^+.[52] The pH influence was considered because the protonation of the imidazole groups (pK_a, ~6.1) in the histidine residue prevents the interaction with metal ions.[53] After incubation with 150 μM of $AgNO_3$ for 30 min at 37 °C, a considerable enhancement (~4.1 fold) of fluorescence was observed in the cells (Fig. 6c and S20†). These results indicate that **2** can penetrate cells and yield a signal for intracellular Ag^+ through the "turn-on" response. Although PA **2** did not include the cell-penetrating peptides, such as TAT, arginine- and lysine-rich peptides,[54] the presence of HG12 on the exterior of the NFs led to cellular uptake of **2** in this condition. It has been reported that the histidine containing peptides can interact with cell membrane *via* electrostatic interactions and permeabilize it under slightly acidic conditions (pH 6.0–7.0).[55] Therefore, the precise mechanism of cell penetration of HG12-containing PAs is being investigated by replacing histidine or glycine with other amino acids. At this stage, we consider that the delicate balance of the characteristic of cationic HG12 located at the corona of NFs and the extent of hydrophobicity of lipid-like alkyl chains may contribute to cellular uptake of NFs of **2**.[56]

The antimicrobial activities of the AgNPs–NFs against both Gram-negative *Escherichia coli* (*E. coli*) O157:H7 and Gram-positive *Bacillus subtilis* (*B. subtilis*) were investigated using growth inhibition assays.[52] The AgNPs, NFs, and AgNP incorporated NFs (AgNPs–NFs) were stored in air for several days and then added to the culture medium, and the turbidity measurements of the cell suspension were taken over a time course (Fig. 7). The bacterial growth rates in Luria–Bertani (LB) liquid media were determined by measuring the optical density at 600 nm (OD_{600}, Fig. 7a). Compared to the growth curve of the control bacteria, the presence of AgNPs–NFs showed a strong inhibition of the growth of *E. coli* O157:H7. In contrast, AgNPs showed a lag phase of 10 h for *E. coli* O157:H7. The bare NFs did not show a noticeable antimicrobial activity against *E. coli* O157:H7, as the curve was similar to that of the control bacteria. After a week, the mixture medium containing the AgNPs–NFs remained pellucid (Fig. 7b), suggesting that few bacteria proliferated in the presence of AgNPs–NFs. These results indicate that the AgNPs decorated on the NFs show potent long-lasting antibacterial activity, since neither the AgNPs nor the NFs inhibited bacterial growth. The assembled microchip device with four unit modules was prepared to further visualize the antimicrobial ability of the AgNPs–NFs (Fig. 7c).[57] The green fluorescent protein (GFP)-expressing *E. coli* O157:H7 solution (OD_{600} = 0.1) suspended in the LB media was introduced into the inlet port in the microchannel using a syringe pump. Four types of microchannels were adopted for loading the control, AgNP, NF, and AgNP–NF solutions, respectively. Fluorescence optical images corresponding to the GFP expression were obtained over time. The innate fluorescence of the NFs was excluded from analysis since the excitation was performed at 488 nm. After incubation for 12 h, the GFP fluorescence appeared in the microchannels loaded with the control and the NF solutions. After 24 h, in all the channels except one channel for the AgNP–NF solution, strong fluorescence emission was observed. These data indicate that AgNPs–NFs exhibit more effective antibacterial activity than AgNPs against Gram-negative bacteria, which is consistent with the results of the turbidity measurements as shown in Fig. 7a. Remarkably, the growth of Gram-positive *B. subtilis* was completely inhibited by the AgNP–NF solution, similar to Gram-negative *E. coli* O157:H7 (Fig. 7d). The observed long-term antibacterial activity of the AgNPs–NFs against both Gram-negative and -positive bacteria is due to their higher stability when compared to the AgNPs. The use of the NF template to guide the growth of the AgNPs and the subsequent formation of hybrid NFs prevent the oxidation and aggregation of AgNPs in air which usually lead to a substantial reduction of antibacterial activity.[58] The demand for novel antibacterial agents has grown significantly in recent years, as the number of infections associated with antibiotic-resistant bacteria has

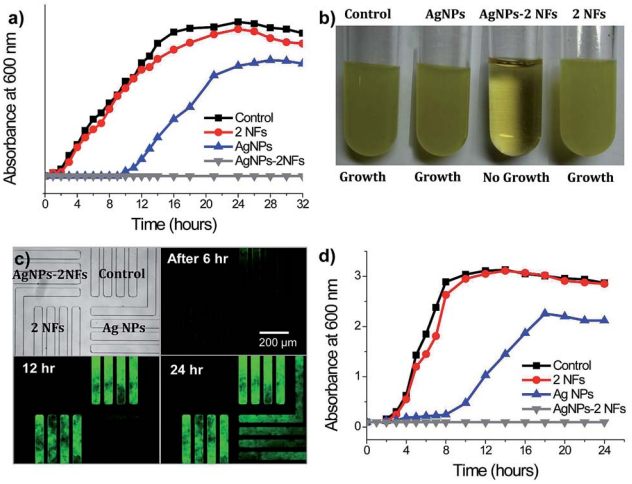

Fig. 7 (a and d) Bacterial growth curves in LB media with the AgNPs–NFs of **2** (10 μg mL^{-1}). The hybrid NFs were added to the culture of (a) *E. coli* O157:H7 or (d) *B. subtilis*. (b) LB liquid medium turbidity assays were employed to evaluate antibacterial activities toward Gram-negative *bacteria E. coli* O157:H7. (c) Optical and fluorescence images (λ_{ex} = 488 nm for GFP) of four types of microchannels for loading AgNP–NF, control, AgNP, and NF solution (clockwise from top left) against bacterial solution (10 μg mL^{-1}), showing different antimicrobial activity over time.

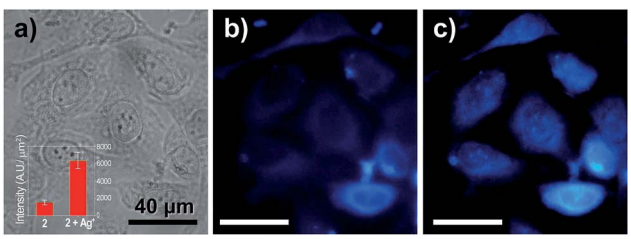

Fig. 6 (a) Bright field and (b and c) fluorescence images of (b) HeLa cells with **2** (10 μM) and (c) PA **2**-loaded HeLa cells in the presence of $AgNO_3$ (150 μM, scale bars: 40 μm). Inset of (a): the intensity of fluorescence per area both before and after incubation with Ag^+.

increased.[59] Therefore, the design and fabrication of AgNP-hybrid 1D NFs based on the aqueous self-assembly of biocompatible PAs may provide a useful approach for the development of antimicrobial nanomaterials as well as for the practical application of supramolecular nanotechnology in health care.

Conclusion

The histidine-rich peptide (HG12)-coated NFs were prepared by the self-assembly of pyrene-labeled PAs in an aqueous solution. As molecular scaffolds, PAs containing linear- or bulky branched alkyl chains were synthesized (for **1** and **2**). The resulting fibrils were similar only outwardly, as they were actually very different. Depending on the number of alkyl chains, different molecular packing arrangements within the NFs appeared, which led to distinct emission modes for the pyrene probe. Even though monomer-like pyrene emission was expressed, the existence of self-assembled NFs enabled the interpretation of the molecular packing within the hydrophobic core in which the pyrene moiety was intercalated between the linear-alkyl chains. Interestingly, the incorporation of branched-alkyl chains into the PA architecture allowed for the loose packing of HG12 on the exterior of the NFs of **2** in an aqueous solution. These molecular packing differences between **1** and **2** resulted in their specific binding affinities to metal ions. The imidazole group of the histidine residue of HG12 acted as a metal binding site, providing a strategy for the fabrication of metal ion-decorated NFs. Both fibrils showed great affinity to Cu^{2+} as a fluorescence "turn-off" sensor. Remarkably, only the NFs of **2** revealed the fluorescence "light-up" response by PET inhibition as Ag^{+} binding. The loose packing distribution of HG12 in the aqueous NFs and the metal ion size requirement for coordination with HG12 contributed to the response to the specific ions and to the maintenance of the fibrillar structure. This characteristic as a supramolecular nanoprobe allows us to identify Ag^{+} in live cells. Furthermore, the outside of the NFs was accessible to serve as a nucleation site for metal nanocrystals. In particular, the AgNPs–NFs showed an enhanced stability of AgNPs in an aqueous solution, which leads to long-term antimicrobial activity against both Gram-negative and -positive bacteria. Considering that a fluorescence "turn-on" chemosensor using the Ag^{+} response has rarely been reported and that novel antimicrobial agents are required to overcome low solubility and stability in aqueous solutions, we believe that this study provides a versatile platform for the creation of supramolecular nanomaterials with optical and biological activities. Since a 1D fibrillar structure is one of the most significant assembly structures for proteins and nucleic acids, this biomorphic mineralization generates further sophisticated strategies for developing advanced materials, including organic–inorganic nanohybrids.

Acknowledgements

This research was supported by the Basic Science Research Program (2011-0014459, 2013R1A2A2A04015914) through the National Research Foundation of Korea (NRF) funded by the Ministry of Science, ICT & Future Planning and Korea Basic Science Institute grant (D34500).

Notes and references

1 (*a*) I. W. Hamley, *Soft Matter*, 2011, **7**, 4122–4138; (*b*) S. Cavalli, F. Albericio and A. Kros, *Chem. Soc. Rev.*, 2010, **39**, 241–263; (*c*) E. Gazit, *Chem. Soc. Rev.*, 2007, **36**, 1263–1269; (*d*) R. V. Ulijn and A. M. Smith, *Chem. Soc. Rev.*, 2008, **37**, 664–675.
2 (*a*) H. Cui, M. J. Webber and S. I. Stupp, *Pept. Sci.*, 2010, **94**, 1–18; (*b*) D. W. P. M. Löwik and J. C. M. van Hest, *Chem. Soc. Rev.*, 2004, **33**, 234–245; (*c*) S. Zhang, *Nat. Biotechnol.*, 2003, **21**, 1171–1178.
3 M. J. Webber, J. Tongers, C. J. Newcomb, K.-T. Marquardt, J. Bauersachs, D. W. Losordo and S. I. Stupp, *Proc. Natl. Acad. Sci. U. S. A.*, 2011, **108**, 13438–13443.
4 J. B. Matson and S. I. Stupp, *Chem. Commun.*, 2012, **48**, 26–33.
5 P. Zhang, A. G. Cheetham, Y.-a. Lin and H. Cui, *ACS Nano*, 2013, **7**, 5965–5977.
6 N. Nuraje, I. A. Banerjee, R. I. MacCuspie, L. Yu and H. Matsui, *J. Am. Chem. Soc.*, 2004, **126**, 8088–8089.
7 I. W. Hamley, *Angew. Chem., Int. Ed.*, 2007, **46**, 8128–8147.
8 (*a*) T. P. J. Knowles and M. J. Buehler, *Nat. Nanotechnol.*, 2011, **6**, 469–479; (*b*) A. W. P. Fitzpatrick, G. T. Debelouchina, M. J. Bayro, D. K. Clare, M. A. Caporini, V. S. Bajaj, C. P. Jaroniec, L. Wang, V. Ladizhansky, S. A. Müller, C. E. MacPhee, C. A. Waudby, H. R. Mott, A. De Simone, T. P. J. Knowles, H. R. Saibil, M. Vendruscolo, E. V. Orlova, R. G. Griffin and C. M. Dobson, *Proc. Natl. Acad. Sci. U. S. A.*, 2013, **110**, 5468–5473.
9 (*a*) T. Koga, M. Matsuoka and N. Higashi, *J. Am. Chem. Soc.*, 2005, **127**, 17596–17597; (*b*) A. Aggeli, M. Bell, L. M. Carrick, C. W. G. Fishwick, R. Harding, P. J. Mawer, S. E. Radford, A. E. Strong and N. Boden, *J. Am. Chem. Soc.*, 2003, **125**, 9619–9628; (*c*) A. Aggeli, I. A. Nyrkova, M. Bell, R. Harding, L. Carrick, T. C. B. McLeish, A. N. Semenov and N. Boden, *Proc. Natl. Acad. Sci. U. S. A.*, 2001, **98**, 11857–11862.
10 S. Zhang, D. M. Marini, W. Hwang and S. Santoso, *Curr. Opin. Chem. Biol.*, 2002, **6**, 865–871.
11 J. D. Hartgerink, E. Beniash and S. I. Stupp, *Science*, 2001, **294**, 1684–1688.
12 L. Hsu, G. L. Cvetanovich and S. I. Stupp, *J. Am. Chem. Soc.*, 2008, **130**, 3892–3899.
13 (*a*) Y.-b. Lim, E. Lee and M. Lee, *Angew. Chem., Int. Ed.*, 2007, **46**, 9011–9014; (*b*) M. O. Guler, S. Soukasene, J. F. Hulvat and S. I. Stupp, *Nano Lett.*, 2005, **5**, 249–252.
14 (*a*) K.-H. Han, E. Lee, J. S. Kim and B.-K. Cho, *J. Am. Chem. Soc.*, 2008, **130**, 13858–13859; (*b*) J.-K. Kim, E. Lee and M. Lee, *Angew. Chem., Int. Ed.*, 2006, **45**, 7195–7198.
15 H. Jiang, M. O. Guler and S. I. Stupp, *Soft Matter*, 2007, **3**, 454–462.
16 D. W. Domaille, E. L. Que and C. J. Chang, *Nat. Chem. Biol.*, 2008, **4**, 168–175.
17 S. N. Dublin and V. P. Conticello, *J. Am. Chem. Soc.*, 2008, **130**, 49–51.

18 M. Murariu, E. S. Dragan and G. Drochioiu, *Biopolymers*, 2010, **93**, 497–508.
19 G. Pappalardo, G. Impellizzeri, R. P. Bonomo, T. Campagna, G. Grasso and M. G. Saita, *New J. Chem.*, 2002, **26**, 593–600.
20 I. A. Banerjee, L. Yu and H. Matsui, *Proc. Natl. Acad. Sci. U. S. A.*, 2003, **100**, 14678–14682.
21 L. Yu, I. A. Banerjee, M. Shima, K. Rajan and H. Matsui, *Adv. Mater.*, 2004, **16**, 709–712.
22 (*a*) C.-L. Chen and N. L. Rosi, *Angew. Chem., Int. Ed.*, 2010, **49**, 1924–1942; (*b*) S. Mann, *Nat. Mater.*, 2009, **8**, 781–792.
23 (*a*) T.-X. Fan, S.-K. Chow and D. Zhang, *Prog. Mater. Sci.*, 2009, **54**, 542–659; (*b*) O. Carny, D. E. Shalev and E. Gazit, *Nano Lett.*, 2006, **6**, 1594–1597; (*c*) E. D. Sone and S. I. Stupp, *Chem. Mater.*, 2011, **23**, 2005–2007.
24 J. D. Tovar, R. C. Claussen and S. I. Stupp, *J. Am. Chem. Soc.*, 2005, **127**, 7337–7345.
25 F. M. Winnik, *Chem. Rev.*, 1993, **93**, 587–614.
26 (*a*) S. Aluri, M. K. Pastuszka, A. S. Moses and J. A. MacKay, *Biomacromolecules*, 2012, **13**, 2645–2654; (*b*) J. L. Pincus, C. Jin, W. Huang, H. K. Jacobs, A. S. Gopalan, Y. Song, J. A. Shelnutt and D. Y. Sasaki, *J. Mater. Chem.*, 2005, **15**, 2938–2945.
27 L. Prodi, F. Bolletta, M. Montalti and N. Zaccheroni, *Coord. Chem. Rev.*, 2000, **205**, 59–83.
28 B. C. Roy, B. Chandra, D. Hromas and S. Mallik, *Org. Lett.*, 2003, **5**, 11–14.
29 (*a*) S. Eckhardt, P. S. Brunetto, J. Gagnon, M. Priebe, B. Giese and K. M. Fromm, *Chem. Rev.*, 2013, **113**, 4708–4754; (*b*) M.-J. Catalina and M. V. H. Eric, *J. Nanopart. Res.*, 2010, **12**, 1531–1551.
30 F. Wang, R. Nandhakumar, J. H. Moon, K. M. Kim, J. Y. Lee and J. Yoon, *Inorg. Chem.*, 2011, **50**, 2240–2245.
31 M. O. Guler, R. C. Claussen and S. I. Stupp, *J. Mater. Chem.*, 2005, **15**, 4507–4512.
32 (*a*) Y. Zheng, Y.-Y. Won, F. S. Bates, H. T. Davis, L. E. Scriven and Y. Talmon, *J. Phys. Chem. B*, 1999, **103**, 10331–10334; (*b*) Z. Li, E. Kesselman, Y. Talmon, M. A. Hillmyer and T. P. Lodge, *Science*, 2004, **306**, 98–101; (*c*) H. R. Marsden, A. V. Korobko, E. N. M. van Leeuwen, E. M. Pouget, S. J. Veen, N. A. J. M. Sommerdijk and A. Kros, *J. Am. Chem. Soc.*, 2008, **130**, 9386–9393.
33 (*a*) S. M. Kelly and N. C. Price, *Curr. Protein Pept. Sci.*, 2000, **1**, 349–384; (*b*) S. Brahms, J. Brahms, G. Spach and A. Brack, *Proc. Natl. Acad. Sci. U. S. A.*, 1977, **74**, 3208–3212.
34 A. Perczel and M. Hollósi, in *Circular Dichroism and the Conformational Analysis of Biomolecules*, ed. G. D. Fasman, Plenum Press, New York, 1986.
35 H. S. Jung, P. S. Kwon, J. W. Lee, J. I. Kim, C. S. Hong, J. W. Kim, S. Yan, J. Y. Lee, J. H. Lee, T. Joo and J. S. Kim, *J. Am. Chem. Soc.*, 2009, **131**, 2008–2012.
36 E. J. Jun, H. N. Won, J. S. Kim, K.-H. Lee and J. Yoon, *Tetrahedron Lett.*, 2006, **47**, 4577–4580.
37 (*a*) M. Nishikawa and K. Ogawa, *Antimicrob. Agents Chemother.*, 2004, **48**, 229–235; (*b*) M. Natali, C. Aakeröy, J. Desper and S. Giordani, *Dalton Trans.*, 2010, **39**, 8269–8277.
38 H.-J. Schneider and A. Yatsimirsky, *Principles and Methods in Supramolecular Chemistry*, Wiley-VCH, Chichester, England, 2000.
39 (*a*) T. Dudev and C. Lim, *J. Mol. Struct.*, 2012, **1009**, 83–88; (*b*) E. Prenesti and S. Berto, *J. Inorg. Biochem.*, 2002, **88**, 37–43; (*c*) K. H. Wu, T. C. Chang, Y. T. Wang, Y. S. Hong and T. S. Wu, *Eur. Polym. J.*, 2003, **39**, 239–245.
40 (*a*) I. Lisiecki and M. P. Pileni, *J. Am. Chem. Soc.*, 1993, **115**, 3887–3896; (*b*) E. Kasotakis, E. Mossou, L. Adler-Abramovich, E. P. Mitchell, V. T. Forsyth, E. Gazit and A. Mitraki, *Pept. Sci.*, 2009, **92**, 164–172.
41 (*a*) C. Salzemann, J. Urban, I. Lisiecki and M.-P. Pileni, *Adv. Funct. Mater.*, 2005, **15**, 1277–1284; (*b*) H.-t. Zhu, C.-y. Zhang and Y.-s. Yin, *J. Cryst. Growth*, 2004, **270**, 722–728.
42 K. Kalyanasundaram and J. K. Thomas, *J. Am. Chem. Soc.*, 1977, **99**, 2039–2044.
43 (*a*) A. P. de Silva, T. S. Moody and G. D. Wright, *Analyst*, 2009, **134**, 2385–2393; (*b*) A. F. Chaudhry, M. Verma, M. T. Morgan, M. M. Henary, N. Siegel, J. M. Hales, J. W. Perry and C. J. Fahrni, *J. Am. Chem. Soc.*, 2010, **132**, 737–747.
44 H. Irving and R. J. P. Williams, *J. Chem. Soc.*, 1953, 3192–3210.
45 J. Yoon, N. E. Ohler, D. H. Vance, W. D. Aumiller and A. W. Czarnik, *Tetrahedron Lett.*, 1997, **38**, 3845–3848.
46 E. Lee, J.-K. Kim and M. Lee, *Angew. Chem.*, 2008, **120**, 6475–6478.
47 (*a*) S. S. Tan, Y. N. Teo and E. T. Kool, *Org. Lett.*, 2010, **12**, 4820–4823; (*b*) K. Rurack and U. Resch-Genger, *Chem. Soc. Rev.*, 2002, **31**, 116–127; (*c*) L. Fabbrizzi, M. Licchelli, G. Rabaioli and A. Taglietti, *Coord. Chem. Rev.*, 2000, **205**, 85–108.
48 (*a*) X.-D. Xu, L. Liang, H. Cheng, X.-H. Wang, F.-G. Jiang, R.-X. Zhuo and X.-Z. Zhang, *J. Mater. Chem.*, 2012, **22**, 18164–18171; (*b*) J. J. Kretsinger, L. A. Haines, B. Ozbas, D. J. Pochan and J. P. Schneider, *Biomaterials*, 2005, **26**, 5177–5186.
49 (*a*) W. Shi, S. Sun, X. Li and H. Ma, *Inorg. Chem.*, 2010, **49**, 1206–1210; (*b*) L. N. Neupane, P. Thirupathi, S. Jang, M. J. Jang, J. H. Kim and K.-H. Lee, *Talanta*, 2011, **85**, 1566–1574.
50 (*a*) Y. Wang, L. Cao, S. Guan, G. Shi, Q. Luo, L. Miao, I. Thistlethwaite, Z. Huang, J. Xu and J. Liu, *J. Mater. Chem.*, 2012, **22**, 2575–2581; (*b*) M. Lv, S. Su, Y. He, Q. Huang, W. Hu, D. Li, C. Fan and S.-T. Lee, *Adv. Mater.*, 2010, **22**, 5463–5467.
51 L. Kvitek, A. Panacek, R. Prucek, J. Soukupova, M. Vanickova, M. Kolar and R. Zboril, *J. Phys.: Conf. Ser.*, 2011, **304**, 012029.
52 J.-M. Kim, C. R. Lohani, L. N. Neupane, Y. Choi and K.-H. Lee, *Chem. Commun.*, 2012, **48**, 3012–3014.
53 (*a*) W.-Y. Chen, C.-F. Wu and C.-C. Liu, *J. Colloid Interface Sci.*, 1996, **180**, 135–143; (*b*) R. J. Sundberg and R. B. Martin, *Chem. Rev.*, 1974, **74**, 471–517.
54 (*a*) F. Heitz, M. C. Morris and G. Divita, *Br. J. Pharmacol.*, 2009, **157**, 195–206; (*b*) M. Lindgren, M. Hällbrink, A. Prochiantz and Ü. Langel, *Trends Pharmacol. Sci.*, 2000, **21**, 99–103; (*c*) R. Roy, D. J. Jerry and S. Thayumanavan, *Biomacromolecules*, 2009, **10**, 2189–2193.

55 (*a*) P. Midoux, A. Kichler, V. Boutin, J.-C. Maurizot and M. Monsigny, *Bioconjugate Chem.*, 1998, **9**, 230–267; (*b*) E. J. M. van Kan, R. A. Demel, E. Breukink, A. van der Bent and B. de Kruijff, *Biochemistry*, 2002, **41**, 7529–7539; (*c*) A. Kichler, C. Leborgne, J. März, O. Danos and B. Bechinger, *Proc. Natl. Acad. Sci. U. S. A.*, 2003, **100**, 1564–1568.

56 A. Nagai, Y. Nagai, H. Qu and S. Zhang, *J. Nanosci. Nanotechnol.*, 2007, **7**, 1–7.

57 H.-H. Jeong, S.-H. Lee and C.-S. Lee, *Biosens. Bioelectron.*, 2013, **47**, 278–284.

58 (*a*) C.-N. Lok, C.-M. Ho, R. Chen, Q.-Y. He, W.-Y. Yu, H. Sun, P. K.-H. Tam, J.-F. Chiu and C.-M. Che, *JBIC, J. Biol. Inorg. Chem.*, 2007, **12**, 527–534; (*b*) R. Kumar and H. Münstedt, *Biomaterials*, 2005, **26**, 2081–2088; (*c*) V. K. Sharma, R. A. Yngard and Y. Lin, *Adv. Colloid Interface Sci.*, 2009, **145**, 83–96.

59 J. T. Seil and T. J. Webster, *Int. J. Nanomed.*, 2012, **7**, 2767–2781.